

A COMPUTATIONAL FRAMEWORK TO MODEL MESENCHYMAL STEM CELL
NUCLEUS MECHANICS USING CONFOCAL MICROSCOPY

by

Zeke Kennedy



A thesis

submitted in partial fulfillment

of the requirements for the degree of

Master of Science in Mechanical Engineering

Boise State University

August 2020

© 2020

Zeke Kennedy

ALL RIGHTS RESERVED

BOISE STATE UNIVERSITY GRADUATE COLLEGE

DEFENSE COMMITTEE AND FINAL READING

of the thesis submitted by

Zeke Kennedy

Thesis Title: A Computational Framework to Model Mesenchymal Stem Cell Nucleus Mechanics Using Confocal Microscopy

Date of Oral Examination: 03 July 2020

The following individuals read and discussed the thesis submitted by student Zeke Kennedy, and they evaluated his presentation and response to questions during the final oral examination. They have found that the student passed the final oral examination.

Gunes Uzer, Ph.D Chair, Supervisory Committee

Clare Fitzpatrick, Ph.D. Member, Supervisory Committee

Mahmood Mamivand, Ph.D. Member, Supervisory Committee

The final reading approval of the thesis was granted by Gunes Uzer, Ph.D., Chair of the Supervisory Committee. This thesis was approved by the Graduate College.

DEDICATION

I would like to dedicate this thesis to my mother Mary Kennedy who raised me and worked to provide me with the best possible future.

ACKNOWLEDGEMENT

I would like to acknowledge the contributions in time, advice, and effort given by my advisor Dr. Gunes Uzer. Additionally, I would like to acknowledge the advice and equipment that was provided to me by Dr. Clare FitzPatrick. I also wish to acknowledge both Joshua Newberg as well as Matthew Goelzer for being willing to work with my research and provide images, AFM data, and advice for my work.

ABSTRACT

The mechanical properties of the cell nucleus are emerging as a key component in genetic transcription. It has been shown that the stiffness of the nucleus in part regulates the transcription of genes in response to external mechanical stimuli. The stiffness has been shown to change as a result of both disease and changes to the external environment. While the mechanical structure of the nucleus can be visually documented using a confocal microscope, it is currently impossible to test the stiffness of the nucleus without a mechanical testing apparatus such as an atomic force microscope. This is problematic in that the use of a mechanical testing apparatus involves deconstructing the cell in order to isolate the nucleus and is unable to provide data on internal heterochromatin dynamics within the nucleus. Therefore, our research focused on developing a computational framework that would allow researchers to model the mechanical contributions of the nucleus specific geometry and material dispersion of both chromatin and LaminA/C within an individual nucleus in order to improve the ability of researchers to study the nucleus. We began by developing a procedure that could generate a finite element geometry of a nucleus using confocal images. This procedure was then utilized to generate models that contained elasticity values that corresponded to the voxel intensities of images of both chromatin and LaminA/C by using a set of conversion factors to link image voxel intensity to model stiffness. We then tuned these conversion factors by running *in silico* atomic force microscopy experiments

on these models while comparing the simulation results to atomic force microscopy data from real world nuclei. From this experiment we were able to find a set of conversion factors that allowed us to replicate the external response of the nucleus. Our developed computational framework will allow future researchers to study the contribution of multitude of sub-nuclear structures and predict global nuclear stiffness of multiple nuclei based on confocal images and AFM tests.

TABLE OF CONTENTS

DEDICATION	iv
ACKNOWLEDGEMENT	v
ABSTRACT.....	vi
LIST OF FIGURES	xi
LIST OF ABBREVIATIONS.....	xii
CHAPTER ONE: INTRODUCTION.....	1
1.1 Motivation.....	1
1.2 Specific Research Goals	1
CHAPTER TWO: BACKGROUND.....	3
2.1 Mesenchymal Stem Cell	3
2.2 Nucleus Mechanosensing Mechanism.....	3
2.3 Nucleus Mechanical Structure	4
2.4 Finite Element Analysis.....	5
CHAPTER THREE: DEVELOPMENT OF METHODS	6
3.1 Microscopy	6
3.1.1 Atomic Force Microscopy	6
3.1.2 Confocal Microscopy.....	6
3.2 Simulation.....	7
3.2.1 Model Geometry Creation	7

3.2.2 Converting Image Voxel Intensity to Modulus of Elasticity	7
3.2.3 Simulation Protocol	8
CHAPTER 4: MANUSCRIPT: “A COMPUTATIONAL FRAMEWORK TO MODEL MESENCHYMAL STEM CELL NUCLEUS MECHANICS USING CONFOCAL MICROSCOPY”	
4.1 Abstract	11
4.2 Introduction	12
4.3 Data Collection, Modeling, and Simulation Setup	13
4.3.1 Measuring Stiffness of intact and LaminA/C depleted cell nuclei ..	13
4.3.2 Mesh generation from confocal scans.....	15
4.3.3 Replicating AFM experiments <i>in silico</i>	17
4.3.4 Determination of the element volume for nucleus models	18
4.3.5 Sensitivity of image noise to element volume	20
4.4 Results	22
4.4.1 Linear relationship between voxel intensity and material property is sufficient for assigning material properties for both chromatin and LaminA/C models	22
4.4.2 Linear conversion model is distinct from a homogeneous model for chromatin	26
4.5 Discussion	29
4.6 Methods and Materials.....	31
4.6.1 Cell Culture	31
4.6.2 Nucleus Isolation	31

4.6.3 Gathering Nucleus Stiffness Data Using AFM.....	32
4.6.4 Nucleus Imaging	32
4.6.5 Response surface datapoint generation.....	32
4.6.6 Conversion factor optimization.....	33
4.6.7 Statistical analysis	33
4.6.8 Data availability	33
CHAPTER FIVE: RESEARCH CONCLUSIONS AND FUTURE DIRECTIONS	40
5.1 Summary of research	40
5.2 Current limitations	41
5.3 Future directions	41
REFERENCES	42

LIST OF FIGURES

Figure 1	Nuclear pores are affected by nucleus deformation ³	4
Figure 2.	siRNA mediated depletion LaminA/C decreases isolated nuclei stiffness.	15
Figure 3.	Generation of image-based nucleus model.	18
Figure 4.	Element size sensitivity analysis.....	20
Figure 5.	Element size error analysis.	22
Figure 6.	Optimization shows linear elasticity relationship.	24
Figure 7.	Optimization data for control nuclei knockdown using linear and exponential conversion factors.	26
Figure 8.	Linear conversion vs homogeneous model for chromatin.....	28
Figure S1.	Image noise.	34
Figure S2.	Material elasticity comparison.....	35
Figure S3.	Chromatin material models.....	36
Figure S4.	Heterogeneous vs homogeneous stress dispersion.	37
Figure S5.	Von-mises stress comparison using stress from each element.	38
Figure S6.	Atomic force microscopy curves.	39

LIST OF ABBREVIATIONS

MSC	Mesenchymal Stem Cell
FEA	Finite Element Analysis
AFM	Atomic Force Microscopy

CHAPTER ONE: INTRODUCTION

1.1 Motivation

Within the cell, the stiffness of the nucleus has been shown to effect genetic transcription effecting both the entrance of transcriptional factors into the nucleus as well as the condensation of heterochromatin^{1,2,3}. This stiffness has been shown to change as a result of both disease and the external environment of the cell⁴. Current methods of studying nuclear stiffness rely on using a mechanical testing apparatus such as an atomic force microscope. This method both fails to capture the internal heterochromatin dynamics of the nucleus as well as requiring the nucleus to be isolated killing the cell and eliminating any ability to study the stiffness of the nucleus in vitro. Therefore, the motivation of this research was to develop a method of studying the stiffness of a specific nucleus without requiring a specialized mechanical testing apparatus in order to enable future research into how the stiffness of the nucleus effects gene transcription.

1.2 Specific Research Goals

Previous research into bone mechanics have utilized the programs Amira, Hypermesh, and Bonemat to develop finite element models of specific bones from CT scans.¹⁴ The first goal of our research was to use these softwares to develop a method of generating a finite element model of a mesenchymal stem cell (MSC) nucleus that mimicked both the external shape as well as the internal heterochromatin geometry of the

original nucleus using confocal microscopy images taken from the nucleus. Once the geometry of the nucleus has been created, the next goal of our research was to attempt to tune the stiffness of this model to mimic the real world properties of the nucleus based on the intensities of the original images. This was done by simulating atomic force microscopy experiments on our models and then comparing the results of our simulations to real world results of the same experiment. The next goal of our research was to use this process on 3 separate sets of images to deduce how consistent this process is across different nucleus imaging sessions.

CHAPTER TWO: BACKGROUND

2.1 Mesenchymal Stem Cell

Mesenchymal stem cells (MSC) are multipotent stem cells that can differentiate into several different lines of cells including osteocytes, chondrocytes, and adipocytes⁵. Within bone tissue, MSC's become osteocytes and aid in the remodeling and creation of bone⁶. The differentiation of MSC's into osteocytes is based on the stiffness of the extracellular matrix that the cell is positioned within¹.

This occurs because of how the extracellular matrix provided by osseous tissue deforms the nucleus.² When an MSC is placed onto an extra cellular matrix, the cell is able to develop focal adhesions to the environment allowing for the cytoskeleton to spread the cell out which pulls at the nucleus causing it to deform^{1,6}. When the cell is on a stiffer environment such as osseous tissue, it is able to form stronger focal adhesions causing greater deformation of the nucleus^{1,6}.

2.2 Nucleus Mechanosensing Mechanism

The nuclear envelope is covered with small pores as shown in figure 1¹. These pores will stretch when the nucleus is deformed. When this occurs, transcriptional growth factors are able to enter the nucleus and then effect cell fate and differentiation¹. Chromatin condensation has also been shown to change due to external nuclear loading⁷. A link exists between chromatin condensing into dense heterochromatin structures and

gene silencing, this link is countered by mechanical stimuli where force induced stretching of chromatin is known to induce transcriptional upregulation of silenced genes^{2,3}.

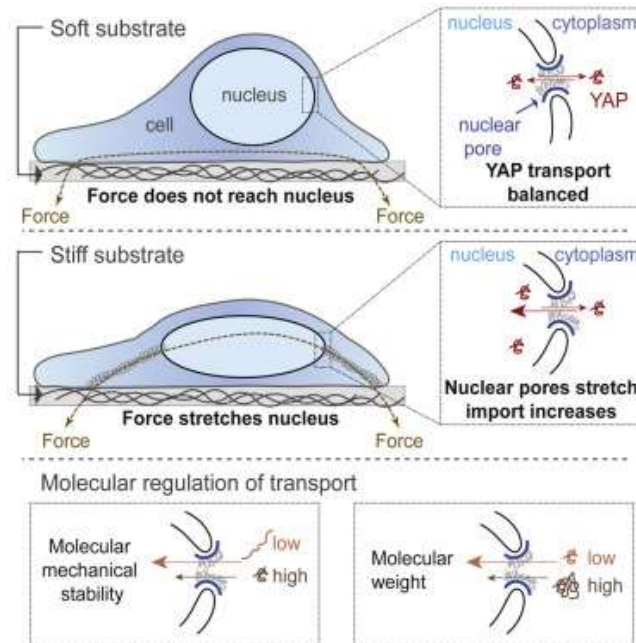


Figure 1 Nuclear pores are affected by nucleus deformation³

2.3 Nucleus Mechanical Structure

Nucleus deformability is affected primarily by Chromatin and LaminA/C⁸.

Chromatin is tightly packed DNA and is present within the nucleus and makes up most of the nucleus's mass⁸. LaminA/C is a protein that lines the nuclear membrane and contributes to the mechanical strength of the nucleus⁹. MSC nuclear LaminA/C levels have been shown to change in response to exposure to disease and environments such as microgravity⁴.

2.4 Finite Element Analysis

Finite element analysis (FEA) is a computerized method of mechanically simulating real world objects. Finite element analysis operates by splitting a geometry of a real-world object into small sections called elements. These elements are made of simplistic shapes that can be mathematically modeled.¹⁰ The geometry would then undergo a simulation of a real world event while the response of each element is recorded and analyzed allowing the user to simulate shapes that are too time consuming or complex for traditional analysis.¹⁰

The element shape selected for this research is the C3D4 tetrahedral element. These elements are made using nodes. Nodes are points in 3D space specified by an x, y, and z position. Elements are a series of nodes that have been linked together to create a geometry. Tetrahedral elements are made using either four or ten nodes. Four noded tetrahedrals have a node on each corner of the tetrahedral while ten noded tetrahedrals have a node on each corner and the center of each edge. Four noded tetrahedrals are more computationally efficient element per element while ten noded tetrahedrals are more accurate at larger sizes but require more computation time.^{11,12}

CHAPTER THREE: DEVELOPMENT OF METHODS

3.1 Microscopy

3.1.1 Atomic Force Microscopy

Atomic force microscopy (AFM) is a method of mechanically measuring a samples' stiffness by measuring the force required to indent the sample.¹³ This is achieved by using a cantilevered probe with a spherical tip attached where the cantilever has a known spring constant as well as a reflective surface at over the contact area of the probe.¹³ When the probe is in use, a laser is shined onto the reflective surface of the cantilever and received by a sectional photodiode.¹³ When this setup pushes on the sample, the cantilever is deformed changing the impact point of the laser upon the photodiode allowing for a calculation of the force exerted using the known spring constant of the cantilever and the angle of deflection of the laser. For our research, the stiffness of isolated MSC nuclei was found using a Bruker Dimension FastScan Atomic Force Microscope (AFM) using a tipless MLCT-D probes with a 0.03 N/m spring constant functionalized with 10 μm diameter borosilicate glass beads.

3.1.2 Confocal Microscopy

Confocal microscopes take 3D images of an object by taking a series of 2D images positioned on top of each other. This is done by centering the microscope on a nucleus then focusing the microscope on the very bottom of the nucleus where an image is taken. The focal height is then raised so that the next layer of the nucleus is in focus

where another image is taken. This process repeats until the entire nucleus has been imaged. For our research, images of MSC nuclei were taken using a Nikon A1 confocal microscope at a rate of .2 μm per image with an image voxel width of .05 μm .

3.2 Simulation

3.2.1 Model Geometry Creation

Models were created by first importing the nucleus confocal images into the Amira software package (ThermoFisher, MA), from this point Amira's segmentation features were used to manually segment the images to isolate the nuclear geometry. Amira's meshing feature was then employed to generate a surface mesh made of triangular S3 elements around the nucleus geometry. This surface mesh was then exported as a .stl file and imported into Hypermesh (Altair Engineering, MI) where it was filled with C3D4 tetrahedral elements creating a volume mesh. This volume mesh was then exported as a .inp file.

3.2.2 Converting Image Voxel Intensity to Modulus of Elasticity

Once the geometry of the nucleus was generated, the finite element model was imported into the Bonemat software package (<http://www.bonemat.org/>) where Bonemat was then used to overlay the volumetric mesh with the original confocal image and assign elasticity values to each tetrahedral element using the average voxel intensity (HU) within each element. For this research, an equation to correlate the image intensity to the modulus of elasticity for the finite element model was created by modifying the equations used within Bonemat. Bonemat uses the equation

$$\rho = a1 + b1 * HU^{c1}$$

to correlate image density to material density and the equation

$$E = a^2 + b^2 * \rho^{c^2}$$

to match material density to element modulus of elasticity.¹⁴ The exact conversion between the density of chromatin and LaminA/C in relation to its image intensity is currently unknown. Due to this we will convert image intensity directly to modulus of elasticity for the chromatin and LaminA/C of the cell using the equation

$$E = a + b * HU^c \quad (1)$$

where a, b, and c are conversion factors used to change an image intensity (HU) into a modulus of elasticity.

3.2.3 Simulation Protocol

Atomic force microscopy simulations were conducted using Abaqus 2019. During simulation, the bottom layer of nodes of the nucleus model was encastered to simulate the nucleus being attached to the plate. A simulated atomic force microscopy tip was formed by positioning a sphere ($r=5 \mu\text{m}$) formed from C3D4 elements with a rigid body material definition above the nucleus model. An encastered node was created and a CONN3D3 connector element was attached between the encastered node and a node on the AFM tip to facilitate the movement of the tip. Contact between the nucleus model and the atomic force microscopy tip was defined as a no friction contact pair between the nodes on the outside layer of the nucleus and the tetrahedral surfaces on the outside layer of the atomic force microscopy tip. During simulation, the connector was expanded lowering the atomic force microscopy tip into the nucleus model until the nucleus model was indented by $1.5 \mu\text{m}$. The force required to expand the connector along with its displacement is recorded and a Matlab code collects the resulting force displacement curve, finds when

the AFM tip contacts the nucleus, and deletes the data before contact and after the first 1 μm of AFM tip after contact.

CHAPTER 4: MANUSCRIPT: “A COMPUTATIONAL FRAMEWORK TO MODEL
MESENCHYMAL STEM CELL NUCLEUS MECHANICS USING CONFOCAL
MICROSCOPY”

Kennedy Z¹, Newberg J¹, Goelzer M¹, Fitzpatrick C¹, Uzer G^{1 †}

¹Mechanical and Biomedical Engineering, Boise State University

† Corresponding Author

Running title: A computational framework to model mesenchymal stem cell nucleus
mechanics using confocal microscopy

Funding support: NASA ISGC NNX15AI04H, NIH R01AG059923, and
5P2CHD086843-03, P20GM109095, P20GM103408 and NSF 1929188.

† Corresponding Author:

Gunes Uzer PhD

Boise State University

Department of Mechanical and Biomedical Engineering

1910 University Drive, MSd-2085

Boise, ID 83725-2085

Ph. (208) 426-4461

Email: gunesuzer@boisestate.edu

4.1 Abstract

Nuclear mechanics is emerging as a key component of stem cell function and differentiation. While changes in nuclear structure can be visually imaged with a confocal microscope, mechanical characterization of nucleus and its sub-cellular components require specialized testing apparatus. A computational model that would permit researchers to gather cell specific mechanical information directly from confocal and atomic force microscopy of cell nuclei would be of great value. Here, we developed a computational framework for generating finite element models of isolated cell nucleus from multiple confocal microscopy scans and simple AFM tests. Utilizing siRNA-mediated LaminA/C depletion, 3D confocal imaging stacks of isolated mesenchymal stem cell (MSC) were converted into finite element models incorporating both chromatin and LaminA/C structures. Using AFM-measured experimental stiffness values, a set of conversion factors were found for both chromatin and LaminA/C to map the voxel intensity of the original images to the element stiffness allowing us to predict nuclear stiffness of other nuclei. The developed computational framework will permit researchers to study the contribution of multitude of sub-nuclear structures and predict global nuclear stiffness of multiple nuclei based on simple nuclear isolation protocols, confocal images and AFM tests.

Key words: Finite Element Analysis, Mesenchymal Stem Cells, Nucleus, Mechanobiology, LaminA/C, Chromatin, Confocal Microscopy

4.2 Introduction

All living organisms function in mechanically active environments by adapting to these challenges at organ, tissue, and cell level. Mesenchymal stem cells are the tissue resident stem cells of musculoskeletal tissue that in-part regulate the adaptive response to mechanical challenge by proliferating and differentiating necessary cell types¹⁵. A major driver of MSC differentiation is the stiffness of the extracellular matrix¹⁶. For example, plating MSCs onto soft and stiff substrates can drive MSC differentiation towards adipogenesis or osteogenesis, respectively⁶. An MSC is able to sense the stiffness of its extracellular matrix by an interplay between focal adhesions, the cytoskeleton, and the nucleus¹. When an MSC is placed onto a stiffer extracellular matrix, the cell will increase the size and number of focal adhesions to the extracellular matrix¹⁷ that serves to generate cell traction along the extracellular matrix¹. As the cell spreads along the extracellular matrix, actin microfilaments tug on the nucleus causing it to stretch and deform¹⁸. These changes in the nuclear structure are critical for the cell function. For example, the nuclear membrane is covered with nuclear pore complexes that are sensitive to deformations of the nucleus. When these pores are opened, the transcriptional factors such as YAP/TAZ are allowed into the nucleus to regulate gene expression¹⁹. Further, chromatin itself was also shown to be responsive to mechanical challenge, as application of mechanical forces alter heterochromatin dynamics and organization^{20,21}. While signaling events such as YAP/TAZ and DNA changes are areas of active research, probing nuclear mechanical properties in living cells remain challenging.

Quantifying the bulk mechanical properties of nucleus can be done through instruments such as atomic force microscopes, micropipette setups, optical tweezers, and

microfluidics²². While single-cell level optical methods to measure intra-nuclear deformations are emerging²³, cellular FE models that can capture nuclear structure and predict nuclear mechanics of many nuclei would be advantageous for time and cost. The stiffness of the nucleus is primarily effected by two nuclear components, LaminA/C that scaffolds the inner nuclear membrane and chromatin⁸. LaminA/C is a protein that lines the nuclear envelope adding mechanical stiffness to the nucleus while Lamin B does not contribute to nuclear mechanics⁹. Chromatin is made of compact DNA and histones that occupies the interior of the nucleus and also provides mechanical competence^{24,25}. Therefore, to model nuclear mechanics these two components are essential.

Here we sought to create a method that can use imaging intensity data from confocal images from LaminA/C and chromatin to directly predict nuclear mechanical properties. In this study we developed a computational framework capable of producing confocal-image based finite element models of an MSC nucleus that could replicate the structural configuration of both chromatin and LaminA/C. Finite element models have been validated by using AFM based measurements on cell nuclei with or without LaminA/C and then replicating the same experiments using a finite element model with image intensity based elasticity values. This model was then used predict the stiffness of two test nuclei based on confocal images alone.

4.3 Data Collection, Modeling, and Simulation Setup

4.3.1 Measuring Stiffness of intact and LaminA/C depleted cell nuclei

As we sought to model nuclear stiffness based on confocal images of LaminA/C and chromatin, we first obtained mechanical properties of cell nuclei isolated from live

MSCs with or without LaminA/C. Two groups of MSCs were cultured in growth media (IMDM, 10 % fetal bovine serum, 1%Pen Strep). One group received a LaminA/C specific siRNA treatment (siLamin) while the other was treated with a control siRNA (siControl). 48h after siRNA treatment, cell nuclei were isolated, plated onto 0.1% Poly-L-Lysine coated plates for adherence and subsequently subjected to atomic force microscopy (AFM) testing to obtain force-displacement curves as we reported previously (**Fig.2a**)²⁶. As shown in immunolabeled nuclei images (**Fig 2b**), isolated nuclei appeared round and maintained intact LaminA/C (red) and DNA (blue) confirmation. Force-displacement curves for siControl and siLamin groups were obtained by indenting the nucleus by 1 μm using a 10 μm diameter spherical borosilicate tip attached to the cantilever beam of the AFM. Shown in **Fig.2c**, the maximum force measured at the AFM tip for the siLamin group on average was 59% smaller than the siControl group ($p < 0.05$), suggesting that nuclei are softer without LaminA/C as indicated in previous research⁹.

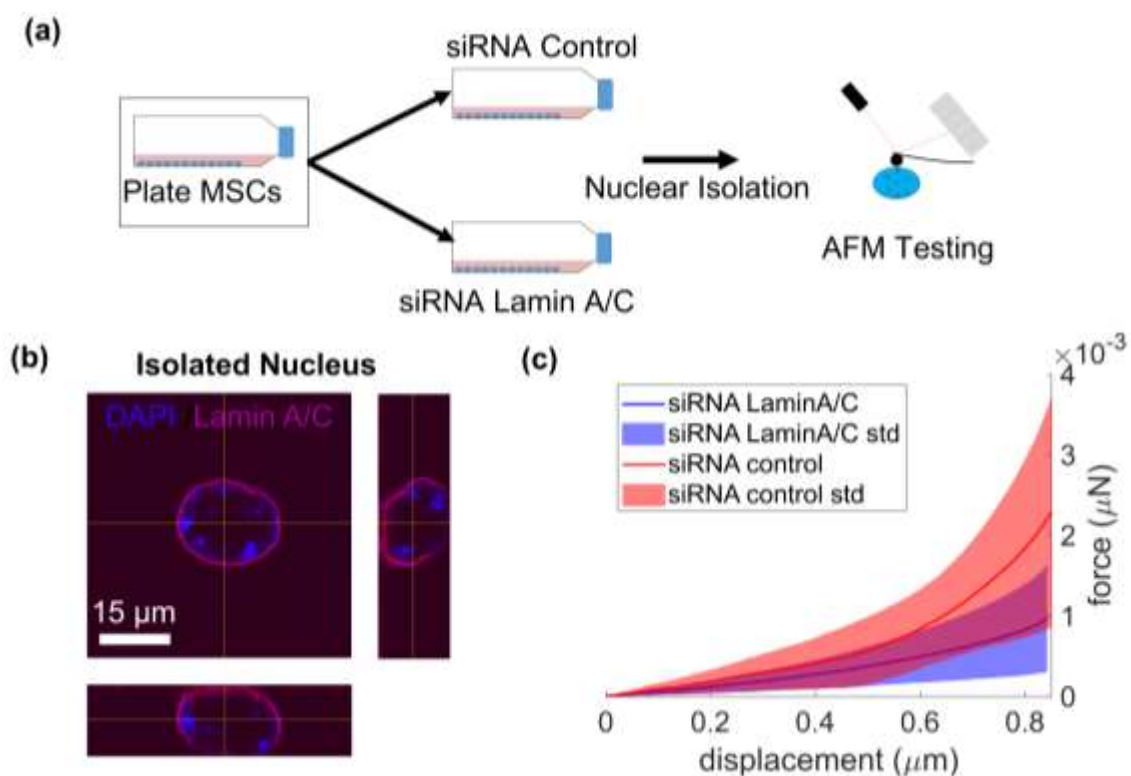


Figure 2. siRNA mediated depletion LaminA/C decreases isolated nuclei stiffness.

a) 2 groups of MSCs are grown in 10 % fetal bovine serum. One of these groups then received a LaminA/C specific siRNA treatment while other was treated with a control siRNA. The nuclei were isolated and subsequently subjected to AFM testing where the nuclei for both the control group (n=30) and the LaminA/C knockdown group (n=73) are indented by 1 μm using a spherical tip with a diameter of 6 μm . b) Confocal microscopy images of a nucleus stained for chromatin (Hoechst 33342) and LaminA/C (cell signaling mAB4777). c) Force-displacement curves from the nucleus indentation average force values for control nuclei (red) and LaminA/C siRNA (blue) were shown as solid lines, standard deviation was shown as shaded area.

4.3.2 Mesh generation from confocal scans

In order to model the contribution of LaminA/C and chromatin separately, we have generated two volumetric meshes for each nucleus image. The first mesh was generated using the DNA signal and the second one was generated using the LaminA/C signal. For chromatin, the 3D confocal image of the chromatin was imported into the

Amira software package (ThermoFisher, MA) and nucleus geometry was manually segmented (**Fig.3a**). A surface mesh made of triangular S3 elements surrounding the nucleus geometry was then created (**Fig.3b**). This surface mesh was then imported into Hypermesh (Altair Engineering, MI) and filled with C3D4 tetrahedral elements to create a volume mesh (**Fig.3c**). Shown in **Fig.3d**, this volume mesh was then imported into the Bonemat software package (<http://www.bonemat.org/>). Bonemat was used to overlay the volumetric mesh with the original confocal image and assign stiffness values to each tetrahedral element using the average voxel intensity (HU) within each element and equation (1) shown below

$$E = a + b * HU^c \quad (1)$$

For this study, term a represented the intensity independent elastic modulus and was set to 0. Terms b and c are a set of conversion factors defined during each experiment. Values for b and c were later assigned in the study based on AFM data. In this study we used a linear isotropic elastic material definition with a Poisson's of 0.5 for each model based on previous literature²⁷. This step is done again for LaminA/C. For this study we have generated LaminA/C and chromatin meshes for 5 nuclei imaged via a Nikon A1 confocal microscope with an image depth of .2 μm and a voxel width of .05 μm .

To generate a model that contains both LaminA/C and chromatin, two identical nucleus geometries were produced. Using the LaminA/C depleted nuclei force-displacement curves, one of the meshes was given elasticity values using the images/conversion factors of chromatin while the other mesh was given elasticity values using the images/conversion factors used for LaminA/C using the AFM data from intact

nuclei. The chromatin and LaminA/C elasticities in each element were then added together to produce one model that contains the elasticity of both materials.

4.3.3 Replicating AFM experiments *in silico*

Atomic force microscopy simulations were conducted using ABAQUS (2019, Dassault Systems, France). Shown in **Fig.3e**, a replica of the AFM test setup was modeled *in silico*. The bottom node layer of the nucleus model (red) was fixed to a rigid plane in all orthogonal directions to simulate the nucleus being attached to the poly-L-Lysine coated plate surface. A simulated AFM tip (yellow) was formed by positioning a sphere ($r=5\ \mu\text{m}$) made of C3D4 elements with a rigid body material definition above the nucleus model. Contact between the outside nodes of the nucleus and the tetrahedral surfaces on the outside layer of the AFM tip was defined as a no-friction contact pair. During simulation, the AFM tip was lowered onto the nucleus until $1.5\ \mu\text{m}$ indentation as shown in **Fig.3f**. The force required to indent the nuclei along with the tip displacement was recorded up to $1.5\ \mu\text{m}$ indentation following contact detection between the AFM tip and the nucleus.

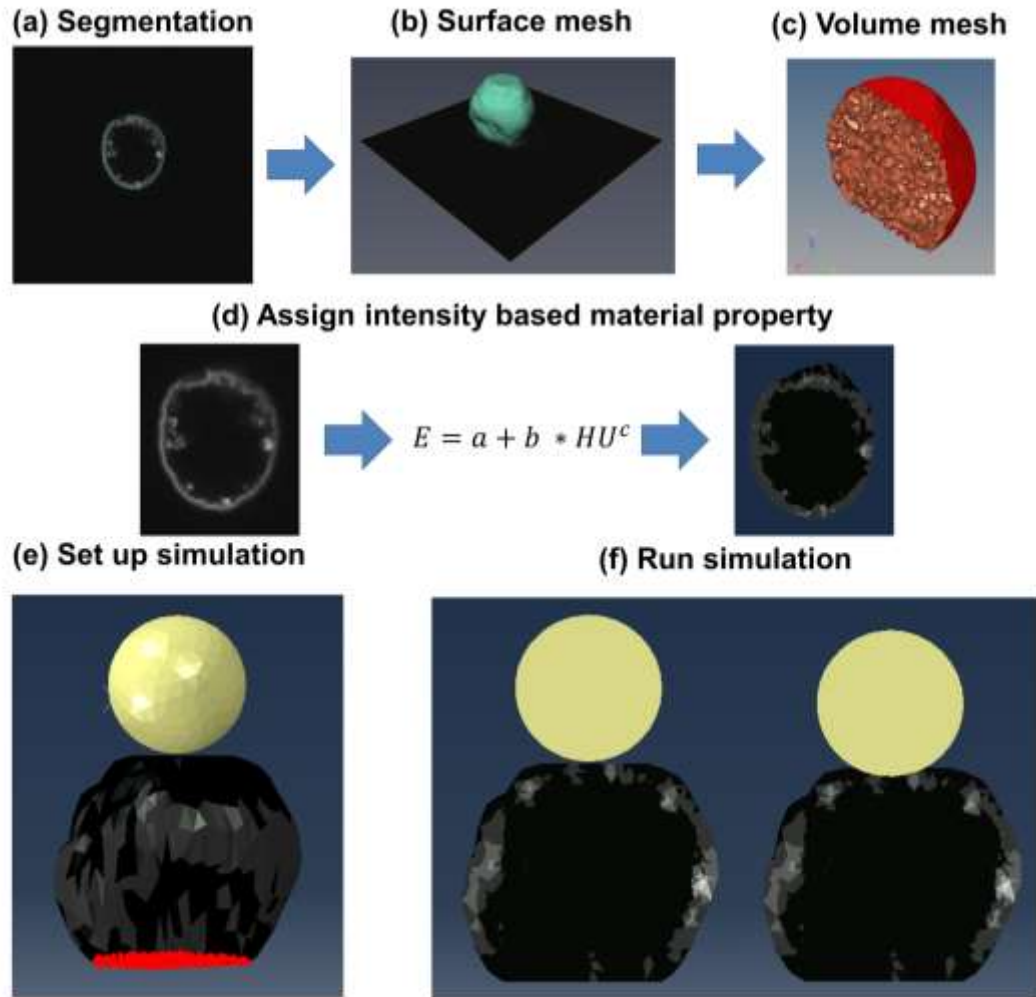


Figure 3. Generation of image-based nucleus model.

a) Images of MSC nuclei are manually segmented using Amira to isolate the nuclear geometry. b) Segmented images are then used to create a surface mesh of the nucleus geometry. c) Surface image is then used to create a volume mesh. d) The volume mesh is then given material properties using the voxel intensity of the original image and equation 1. e) Image of simulated atomic force microscopy experiment with AFM tip (yellow) heterogeneous nucleus (blue) and encastered base nodes (red). f) Images of simulated nucleus compression with a normal experiment before indentation (left) and after indentation (right).

4.3.4 Determination of the element volume for nucleus models

In order to determine the sensitivity of AFM indentation force to mesh element volume, nucleus models were constructed from 5 chromatin nuclei images with element volumes of 5, 4, 3, 2, 1, .8, .6 μm^3 . The models were then given elasticity values using

their original chromatin images using conversion factors $a = 0$, $b = 20$, and $c = 1$ with a set to 0 under the assumption that there is no base elasticity independent of image intensity, b set to 20 to increase the amount of different materials within Bonemat and c set to 1 to scale elasticity linearly to image voxel intensity. A representative image for nuclei #1 meshes with varying element volumes along with the original images at each orthogonal mid-orthogonal plane was depicted in **Fig.4a**. Each nuclei model was then subjected to *in silico* AFM experiments. The force generated at 1 μm of nuclei model indentation was recorded from each simulation and the evolution of maximum force was plotted against element volume for each nucleus. As shown in **Fig.4b**, mean value was represented by solid line and standard deviation was represented by red shaded area. Compared to 5 μm^3 , mean maximum force value and standard deviation started to plateau after 1 μm^3 indicating the volume that can be used without affecting the maximum force output (green line).

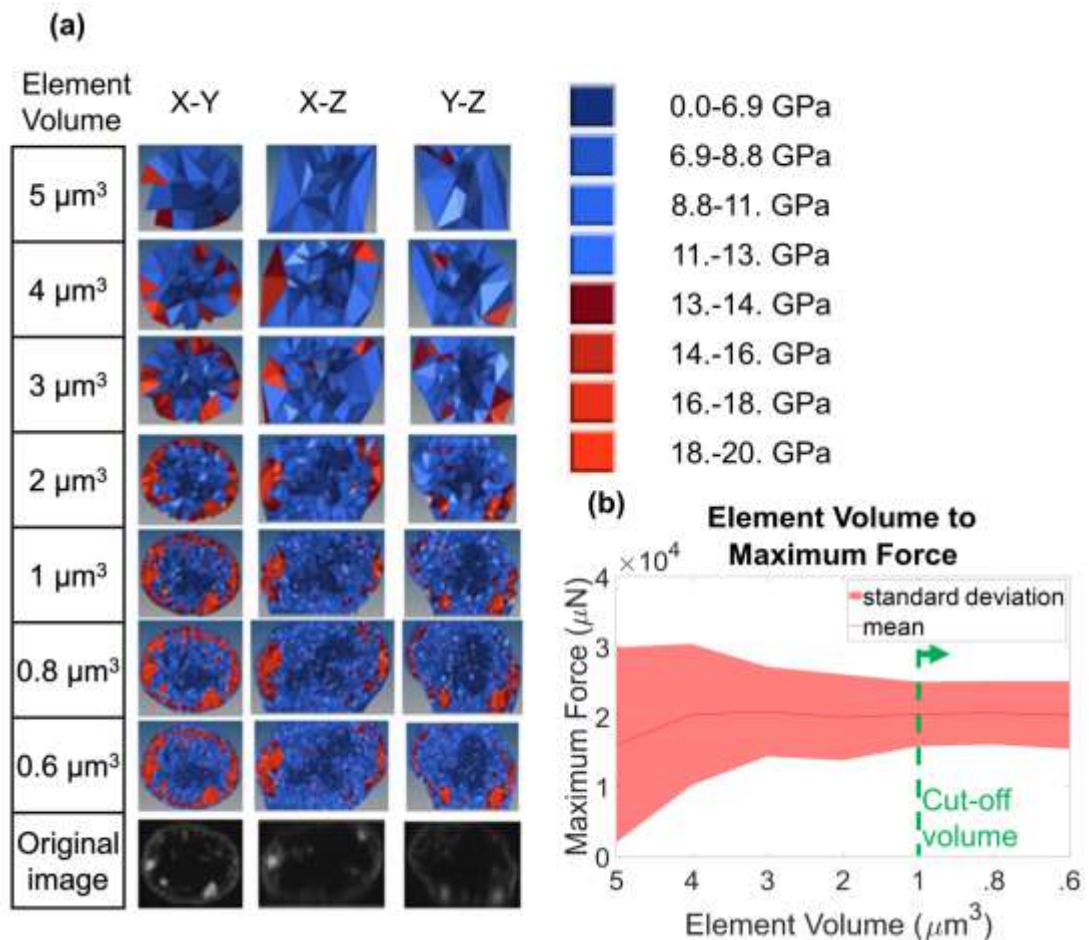


Figure 4. Element size sensitivity analysis.

a) Cross sectional images of nuclei models created with elements that have an average element size of 5, 4, 3, 2, 1, .8, .6, and .3 μm^3 . Material parameters were set to $b=20$ kPa and $c=1$. Color maps indicate corresponding stiffness values. b) Graph of how maximum force, measured at the AFM tip pressing on to the nucleus, versus the element size averaged for three nuclei. Solid line represents mean and shaded area indicates standard deviation. Element sizes smaller than 1 μm^3 does not affect maximum force and standard deviation (green dashed line).

4.3.5 Sensitivity of image noise to element volume

While force sensitivity analysis revealed a cut-off at 1 μm^3 , we sought to quantify how well element volumes represented the spatial information from confocal images, as this may be important for discerning nuclear deformation patterns. To accomplish this, chromatin images for a single nuclei image (Nuclei #1) was converted into 6 finite element models meshed with average element sizes of 3, 2, 1.5, 1, .8, .6, and .3 μm^3 and

given elasticity values using the conversion factors $a = 0$, $b = 20$, and $c = 1$. A Matlab script then extracted a 3D image from each mesh with the 2D image from a transverse plane ($Z=7 \mu\text{m}$) visible within **Fig.5**, top row.

These images were then overlaid with the original image (**Fig.5**, second row) and the intensity of each voxel was compared to each voxel in the original image, producing a color map indicating the percent differences (**Fig.5**, third row). Microscopy noise in the confocal images was accounted for by comparing the average intensity of the DNA free region of interest to each voxel with that region (**Fig.S2**). This analysis produced an average error value of 13%, indicating the amount of inherent noise in the confocal images. This value was then subtracted from each voxel in order to quantify the non-noise related error. These corrected voxel errors were then averaged to generate a final error value (**Fig.5**, bottom row). At $3 \mu\text{m}^3$ element volume the average % error was 12.3%, as element size decreased % error also continued to decrease. At $1 \mu\text{m}^3$ average % error was 6.4%. Beyond $1 \mu\text{m}^3$ and until $0.3 \mu\text{m}^3$ average % error only changed by 1.9% indicating a similar cut off range where $1 \mu\text{m}^3$ voxel volume can represent the 93.6% of the chromatin configuration.

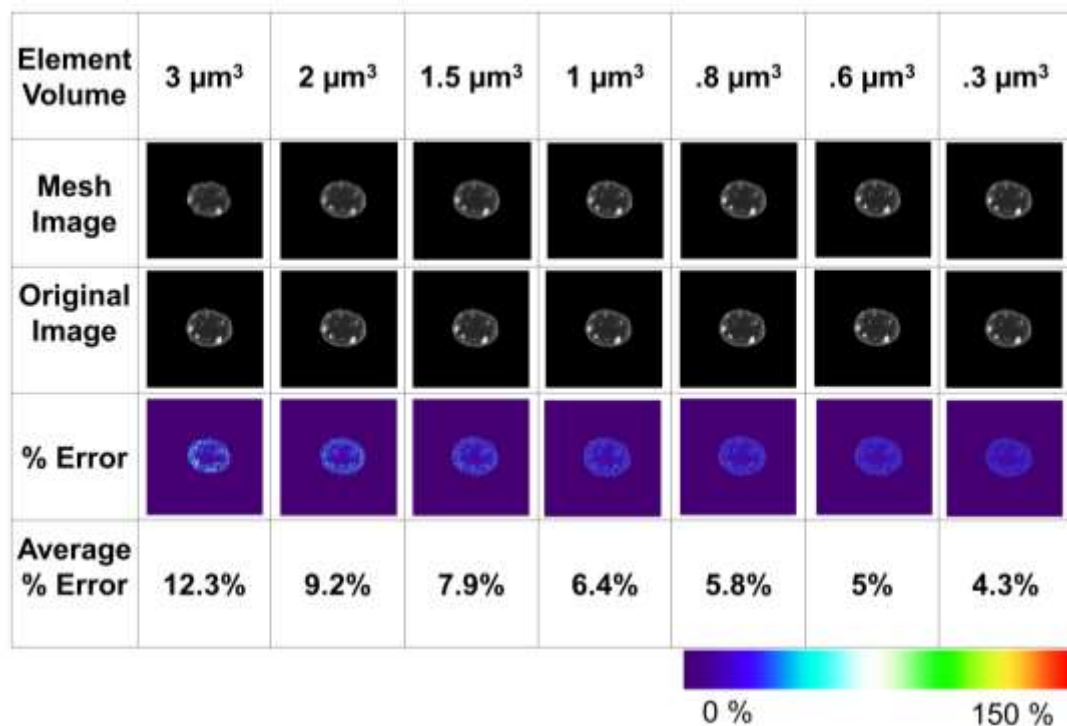


Figure 5. Element size error analysis.

Representative sagittal plane images with the element volumes of 3, 2, 1.5, 0.8, 0.6, and 0.3 μm^3 (2nd row) were compared against the matching location in the original confocal image (3rd row). Quantification of the pixel by pixel intensity values were represented by a % change heat map (4th row). Average % error in 3 and 0.3 μm^3 were 12.3% and 4.3%, respectively.

4.4 Results

4.4.1 Linear relationship between voxel intensity and material property is sufficient for assigning material properties for both chromatin and LaminA/C models

To find the best set of conversion factors to create nuclei models containing chromatin, we generated different nucleus models using different b - c combinations and subjected them to *in silico* AFM tests. As shown in **Fig.6a**, an 8 X 8 response surface was generated to compare the simulated AFM results to experimental AFM data for the LaminA/C depleted nuclei. The b values used were logarithmically spaced between 1×10^{-9} $\mu\text{N}/\mu\text{m}^2$ and 1×10^{-3} $\mu\text{N}/\mu\text{m}^2$ and c values were linearly spaced between 0.5 and 5. The

error associated with each b - c combination was found by generating root mean squared error between simulated and experimental AFM data. Results showed that for every c value there was a b value that minimized the error. In order to expand on this finding, we selected the two c values 0.5 and 1.1 that produced a minimum value within our original 8 X 8 grid (green dotted boxes). Shown in **Fig.6b**, plotting a refined 10 X 10 response surface around these two b - c values, a minimum error along a straight line for different b values was visible (dotted red lines), suggesting that minimizing the error was independent of the initial c value. Shown in bottom right, setting $c=1$ produced a similar set of b values that minimized the error between the simulated and the real AFM experiments, indicating that a linear conversion between pixel intensity and modulus of elasticity could be used.

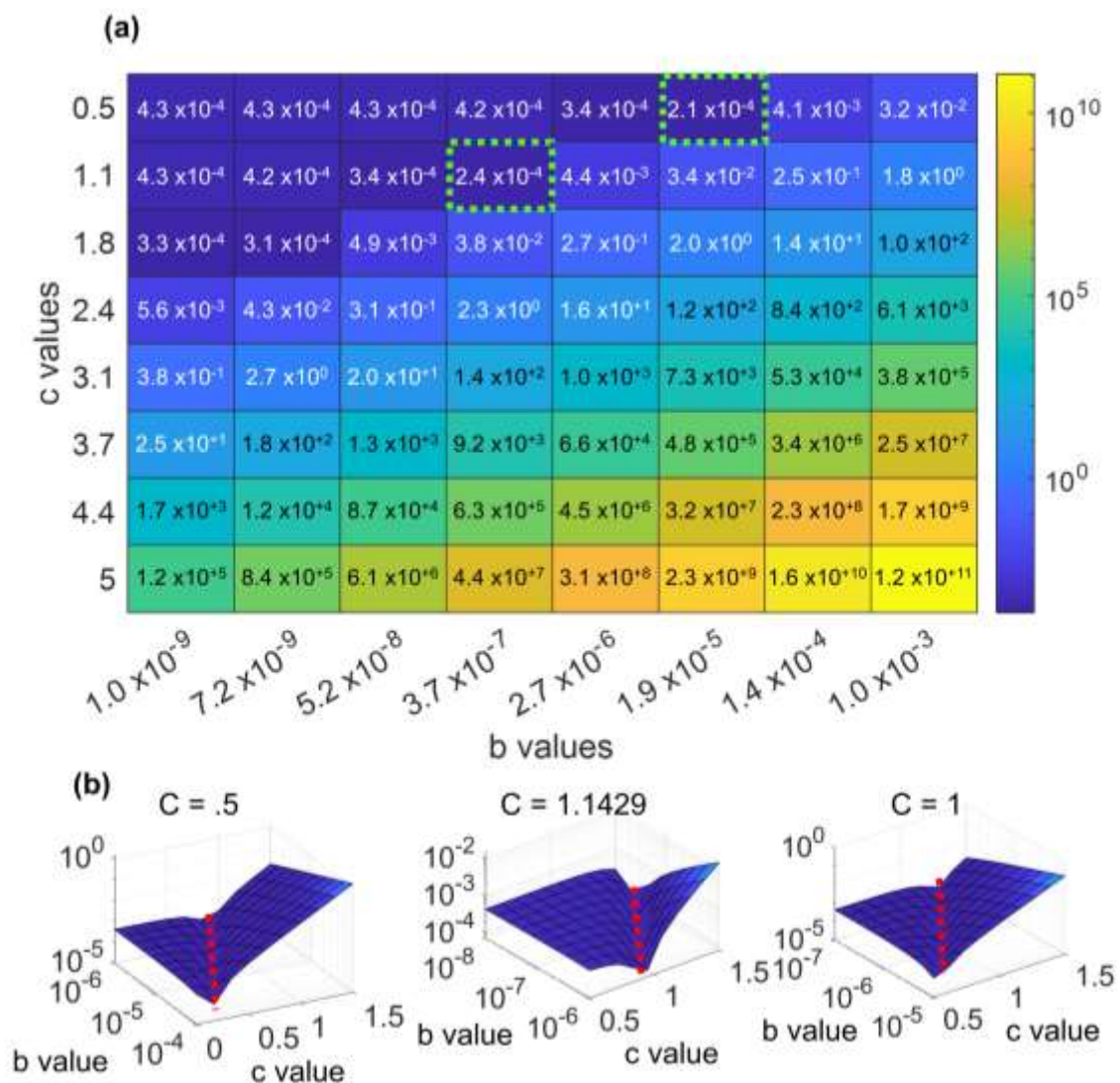


Figure 6. Optimization shows linear elasticity relationship.

a) Error surfaces for 3 LaminA/C depleted nuclei show a rut like error when using different b and c values. b) Higher resolution error surfaces were then done around the lowest points of the original surface, these error surfaces produce minimum values around 10^{-4} similar to the error surface generated around $c=1$ showing that there is a correlation between b and c .

Repeating the same procedure for LaminA/C using chromatin+LaminA/C

combined models and intact nuclei AFM data exhibited a similar material outcome. An 8 X 8 response surface was made for LaminA/C conversion factors that used b values

logarithmically between $1 \times 10^{-9} \mu\text{N}/\mu\text{m}^2$ and $1 \times 10^{-3} \mu\text{N}/\mu\text{m}^2$ and c values linearly spaced

between 0.5 and 5. We again selected two c values 0.5 and 0.14 that produced a minimum value within our original 8 X 8 grid (green dotted boxes). For the first minimum value a 10 X 10 surface centered on $b = 3.7 \times 10^{-7} \mu\text{N}/\mu\text{m}^2$ and $c = 1.1$ was generated. For the second minimum we created a surface centered on $b = 1.9 \times 10^{-5} \mu\text{N}/\mu\text{m}^2$ and $c = 0.5$. Both surfaces show a minimum error along a straight line for different b values (dotted red lines). Comparing with these values another 10 X 10 surface centered on $b = 1 \times 10^{-7} \mu\text{N}/\mu\text{m}^2$ and $c = 1$ was also showed a similar pattern, indicating that a linear relationship between voxel intensity and material property is also sufficient for Lamin A/C. We then set $c=1$ and used the matlab algorithm “fmincon” optimization algorithm with a step tolerance set to 1×10^{-9} to find the b values that minimized the root mean square error for three “training nuclei (nuclei 1,2 and 3) for both chromatin and LaminA/C. This resulted in an optimized b value of $6.3 \times 10^{-7} \mu\text{N}/\mu\text{m}^2$ with an error of $5.5 \times 10^{-5} \mu\text{N}/\mu\text{m}^2$ for chromatin. For LaminA/C the b mean value was $8.64 \times 10^{-7} \mu\text{N}/\mu\text{m}^2$ with an error of $3.1 \times 10^{-4} \mu\text{N}/\mu\text{m}^2$.

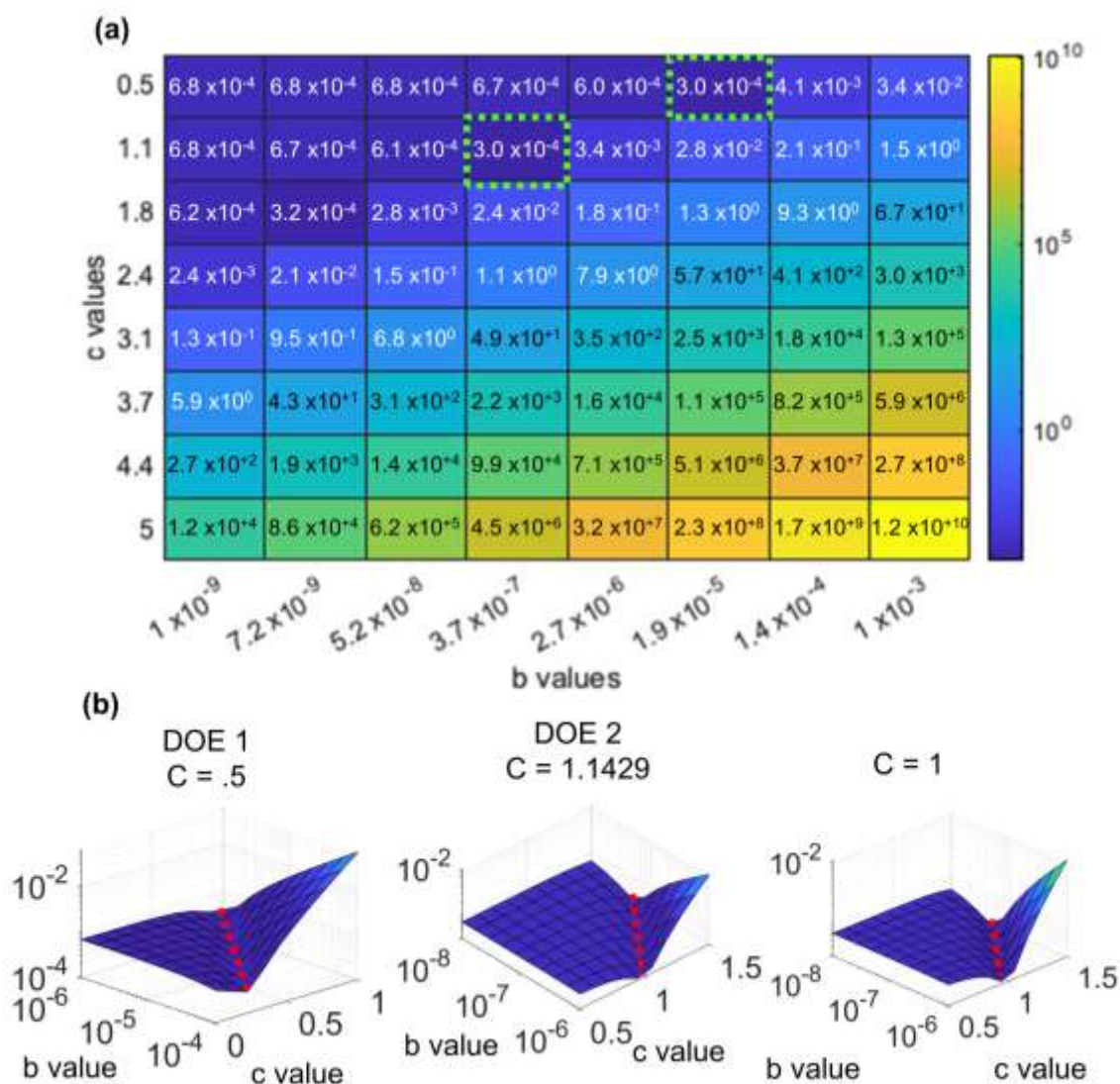


Figure 7. Optimization data for control nuclei knockdown using linear and exponential conversion factors.

a) Error surfaces for 3 control nuclei show a rut like error when using different b and c values. b) Higher resolution error surfaces were then done around the lowest points of the original surface, these error surfaces produce minimum values around 10^{-4} similar to the error surface generated around $c=1$ showing that there is a correlation between b and c.

4.4.2 Linear conversion model is distinct from a homogeneous model for chromatin

To test the differences between homogeneous and linear-elastic heterogenous models, homogeneous chromatin models were made from the chromatin channels of nuclei #1-#3 by setting all the elements to the same elastic modulus. The modulus value

was determined via minimizing the rmse difference between the load-displacement curves of the *in silico* and experimental AFM data of LaminA/C depleted nuclei. This produced a modulus of elasticity of $2.7 \times 10^{-4} \mu\text{N}/\mu\text{m}^2$ with a rmse value of $6.2 \times 10^{-5} \mu\text{N}/\mu\text{m}^2$ with no statistical difference between the error of the homogeneous and linear-elastic heterogeneous models ($p=.83$). Similarly, applying the error-minimized b values to homogenous and heterogeneous models generated from test nuclei (#4 and #5) resulted in rmse values of $6.2 \times 10^{-5} \mu\text{N}/\mu\text{m}^2$ and $5.5 \times 10^{-5} \mu\text{N}/\mu\text{m}^2$ with similar error values ($p=.63$) suggesting that the bulk nuclei response can be modeled using either homogenous or heterogeneous models (**Fig. 8a-b**).

Next, *in silico* cross-sectional von-mises stress during $1 \mu\text{m}$ tip indentation was compared between the homogeneous and heterogeneous models of nuclei #4 and #5. Average von mises stresses at mid-sagittal planes were plotted and compared across a $1 \mu\text{m}$ region of interest located between nuclear heights $Z=5 \mu\text{m}$ and $Z=6 \mu\text{m}$. As shown in **Fig.8c**, heterogeneous models of nuclei #4 (top) and #5 (bottom) showed higher peaks at the nuclear periphery of the region of interest. Quantification of the peripheral peak stresses showed 16% higher stresses in heterogeneous models when compared to homogenous model ($p<0.001$). Von-mises stress values within nuclei #4 and #5 were then compared between homogeneous and heterogeneous models using the stress values within all of the elements as shown in **Fig.S5** where the heterogeneous models showed similar average stresses ($p>.05$) as homogeneous models throughout the bulk of the nucleus suggesting that both materials can model the external stiffness of the nucleus.

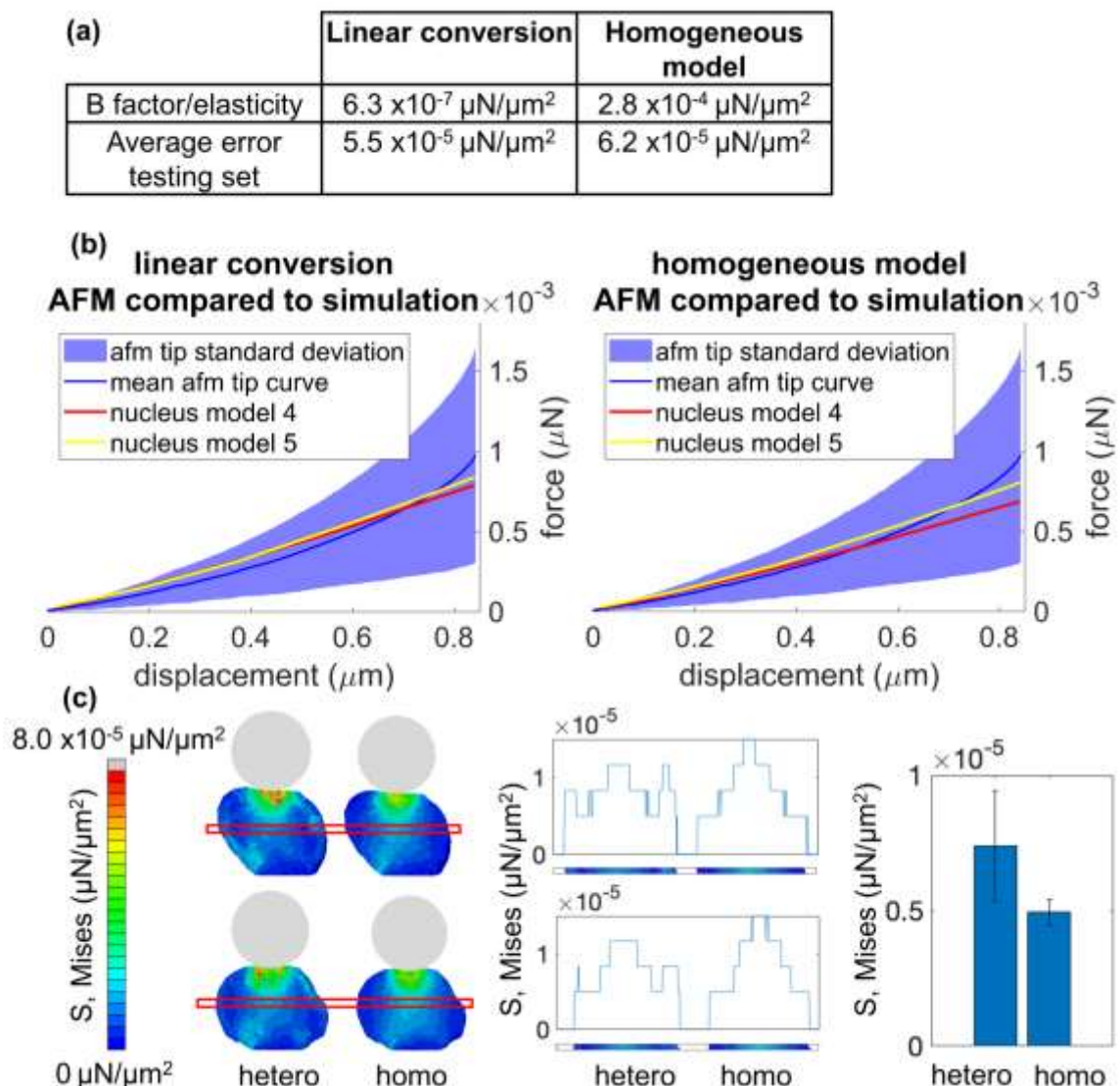


Figure 8. Linear conversion vs homogeneous model for chromatin.

a) Data collected during optimization of the conversion factors displaying both the conversion factor as well as the error for the testing set of nuclei. b) The simulated force curves were then overlaid with the LaminA/C KO results showing the resulting force curves from the linear conversion (left) compared to the results of the homogeneous model (right). c) cross sections of the model at full compression were then imaged (left) and the average stresses within a $1 \mu\text{m}$ tall region beginning at a height of $Z=5 \mu\text{m}$ were plotted (middle), the stresses within the outer 25 percentile of both nuclei was then plotted within a bar plot (right) showing the difference between the stress distributions within the homogeneous and heterogeneous models.

4.5 Discussion

Deformation of the nucleus regulates gene transcription via altering both DNA confirmation²⁸ and the nuclear entry of transcription factors such as YAP/TAZ²⁹. Nuclear deformation in response to mechanical forces is in part controlled by the mechanical stiffness provided by the chromatin and LaminA/C within the nucleus⁸. The computational framework we have generated here is able to capture both geometrical and structural inhomogeneities of both LaminA/C and chromatin from confocal images. Using AFM-calibrated linear voxel-intensity to elastic modulus constants, mechanical behavior of nuclei images were predicted. The inherent limitation of this approach is that before predicting the nuclear mechanical properties, one needs to have a relatively large sample size sets for both AFM and confocal images. Further, while it was outside of the scope of the current study, error associated with experiment to experiment variation of confocal imaging will need to be further evaluated in future studies. Finally, in order for these predictions to be accurate, nuclei has to be isolated from the cell as the cytoskeletal contribution to AFM tests cannot be avoided in intact cells. Even with these limitations this method allows researchers to predict nuclear stiffness and intra-nuclear deformation with only a simple nuclear isolation protocol and confocal imaging. These models of isolated, standalone nuclei developed here will also be important in developing intact cell models in the future.

Our model provides a number of advantages over finite element analyses of the cell nucleus that tend to model the nucleus as a homogenous material properties with idealized geometry.^{30,31} While comparisons between homogenous and heterogenous nuclear structures showed no big changes in “bulk” structural response under in silico

AFM experiments, stresses throughout the nuclear structures were different where stresses concentrations were dependent upon the chromatin and LaminA/C distribution density within the original images (**Fig.8**). As chromatin condensation has been shown to change due to external nuclear loading³², these models may provide useful predictions on what regions of chromatin are experiencing larger loads. Another advantage of the model is the incorporation of nuclear envelope proteins into the model. In this study we have included LaminA/C. The levels of LaminA/C levels has been shown to change under microgravity⁷. This model can potentially predict the nuclear stiffness change due to alterations in LaminA/C levels. Further, the structural contributions of other nuclear envelope proteins such as nuclear pore complexes can also be incorporated into these models in the future, providing a robust computational framework for studying the forces on certain nuclear proteins.

Previous research described the nucleus's mechanical elasticity as either linear elastic or hyperelastic²⁷. During our experiments we chose to model the nucleus as a linear elastic. As both homogenous and linear conversion models of nucleus #4 and #5 produced linear force-displacement curves, we have also implemented hyperplastic Mooney-Rivlin and Neo-Hookean material definitions²⁷ which again produced linear force-displacement relationship (**Fig.S2**). Suggesting that the shape of *in silico* loading curves were independent of the use of hyperelastic Mooney-Rivlin and Neo-Hookean models. Corroborating these *in silico* findings, as shown in Fig.S6, 38% of the AFM-tested nuclei showed linear loading curves.

In summary, our data indicate that that it is possible to generate individual finite element models of nuclei. We have shown that these models could be tuned to match

AFM results of a homogeneous nuclear structure. We have also shown that if a proper relation between chromatin stiffness and image intensity were to be found through external means, our method can then be used to model the internal chromatin dynamics within the nucleus. Our findings may lead to more effective techniques to understanding mechanobiological phenomenon within the cell and improve the study of how cells can adapt to their mechanical environment.

4.6 Methods and Materials

4.6.1 Cell Culture

MSCs were harvested from the bone marrow of 8-wk old male black mice as previously described^{2,3}. Cells were used for experiments were between passage 7 and passage 11. Cells were sub-cultured at the density of 1,800 cells/cm² and maintained within IMDM (12440053, GIBCO) with 10% FCS (S11950H, Atlanta Biologicals) with 1% Pen/strep (GIBCO).

4.6.2 Nucleus Isolation

MSCs were scraped free from their plates using 9 mL of 1x PBS and centrifuged at 1100 RPM at 4°C with a Beckman Coulter Allegra X-30R Centrifuge. MSCs were then suspended within 500 µL hypotonic buffer A (.33M Sucrose, 10mM HEPES, pH 7.4, 1mM MgCl₂, 0.5% w/v Saponin) and centrifuged twice at 3000 RPM, 4°C for 10 minutes using a Beckman Coulter Microfuge 20R Centrifuge. Cytoplasmic supernatant was then aspirated away and the remaining nuclei were then resuspended using 100 µL of hypotonic buffer A. Cytoplasmic debris was then separated from the nuclei by adding 400 µL of Percoll and centrifuging the resulting mixture at 10,000 RPM at 4°C for 10

minutes. Nuclei were then plated in a .01 Poly-L-Lysine coated 35 mm cell culture dish and incubated for 25 minutes.

4.6.3 Gathering Nucleus Stiffness Data Using AFM

A Bruker Dimension Fastscan AFM functionalized with a 10 μm diameter borosilicate glass bead was then used to indent nuclei from the LaminA/C knockdown group (n=73) and the control group (n=30). Compression data was then processed using the software “Nanoscope” where force data before the point of tip contact on the nucleus was deleted. This data was then processed using Matlab to create a curve of points that reflects the mean of the force to displacement curve as well as the standard deviation of the atomic force microscopy experiments.

4.6.4 Nucleus Imaging

A single group of MSC was grown within control conditions and isolated using the methods described above. The chromatin of the nuclei was then stained with Hoechst 33342 while the LaminA/C was stained with mAB 4777 (Abcam). 5 nuclei were then imaged using a Nikon A1 confocal microscope at a rate of .2 μm out of plane and .05 μm in plane resolution.

4.6.5 Response surface datapoint generation

All 5 nuclei confocal microscopy scans were converted to finite element models with an average element size of 1 μm^3 . Each model was then given elasticity values using their original image and the conversion factors of that datapoint. All 5 nucleus models then underwent a simulated atomic force microscopy experiment where force/displacement curves data from the first 1 μm of nuclei indentation was collected. The resulting force displacement curves were then compared to the mean atomic force

microscopy curve taken from the experimental AFM indentations using root mean squared error. The root mean squared error between all 5 of the models were then averaged to create each point of the response surface.

4.6.6 Conversion factor optimization

Nucleus models #1, #2, and #3 were selected and converted to finite element models with an element volume of $1 \mu\text{m}^3$. The c value was then constrained to either $c = 1$ for linear material conversion or $c = 0$ for homogeneous material value while a value of $b = 1\text{E-}10 \mu\text{N}/\mu\text{m}^2$ was used as a starting point. The matlab algorithm “fmincon” was then set to use an “SQP” optimization algorithm with constraint and step tolerance set to $1 \times 10^{-9} \mu\text{N}/\mu\text{m}^2$. This algorithm then optimized the b value by using the b value to generate an error data point using the three nuclei while change the b value until the optimization constraint/step tolerance was met.

4.6.7 Statistical analysis

Results are presented as mean \pm SD unless indicated in figure legends. For comparisons two sample t-test was used. P-values of less than 0.05 were considered significant.

4.6.8 Data availability

The datasets generated and/or analyzed during the current study are available from the corresponding author on reasonable request.

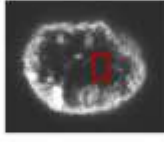
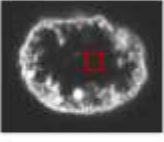
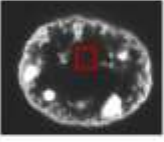
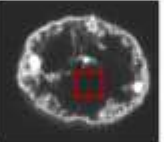
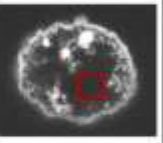
Image noise data					
	1 st area	2 nd area	3 rd area	4 th area	5 th area
Image of area selected					
Area average error	14.%	13.%	13.%	12.%	13%
Total average error	13.%				

Figure S1. Image noise.

5 confocal images of chromatin from nucleus 1 were separated and a homogeneous section of the image was then selected from each image. This section was then used to quantify the image noise within the microscope by finding the average voxel intensity within the images and comparing this value to the voxels within each area. The error between the average voxel intensity and the accompanying area voxels was then averaged to produce an average error of each area. This data was then averaged to produce the average noise within the chromatin image of nucleus 1.

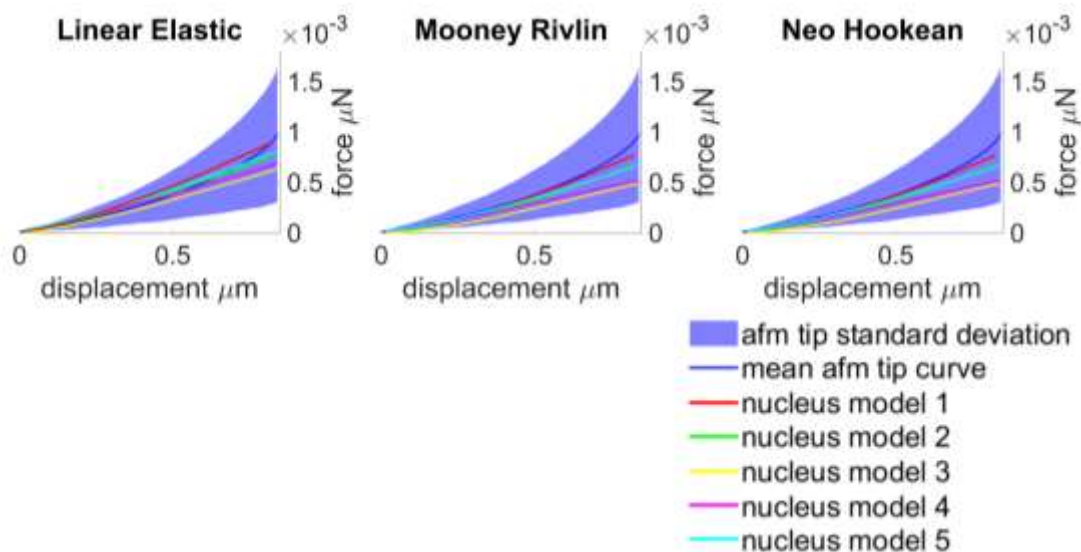


Figure S2. Material elasticity comparison.

Nuclei simulations of nucleus 4 and 5 were attempted using linear isotropic model that used the optimized values for the homogeneous image conversion(left). Mooney-Rivlin models were then created by converting the homogeneous optimized elasticity to Mooney-Rivlin constants as indicated within previous research²⁵ by where c_{01} was set to 0 and c_{10} was formed by dividing the linear isotropic elasticity by 6(middle). From this point, 5 nuclei were formed by creating a Neo-Hookean material model by dividing the homogeneous optimized elasticity by 6 to form the Neo Hookean material constants as explained within the Abaqus source page.

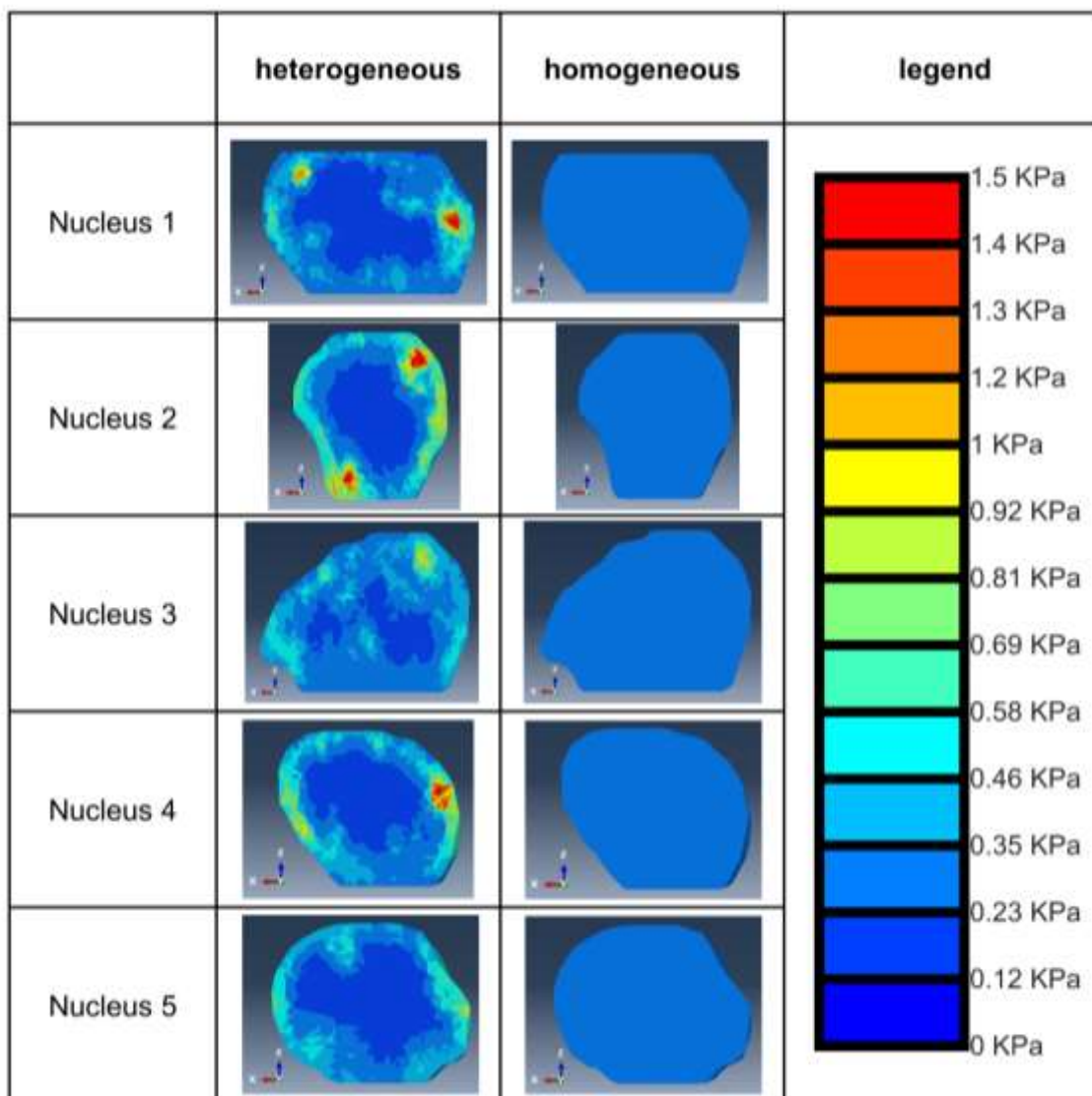


Figure S3. Chromatin material models.

Finite element models of the nucleus have been defined with the chromatin images using both the homogeneous conversion factors and the heterogeneous conversion factors with a cross section of the nucleus models defined with the heterogeneous model shown on the left and cross sections of the homogeneous models shown on the right showing the material values using a color scale shown on the far right.

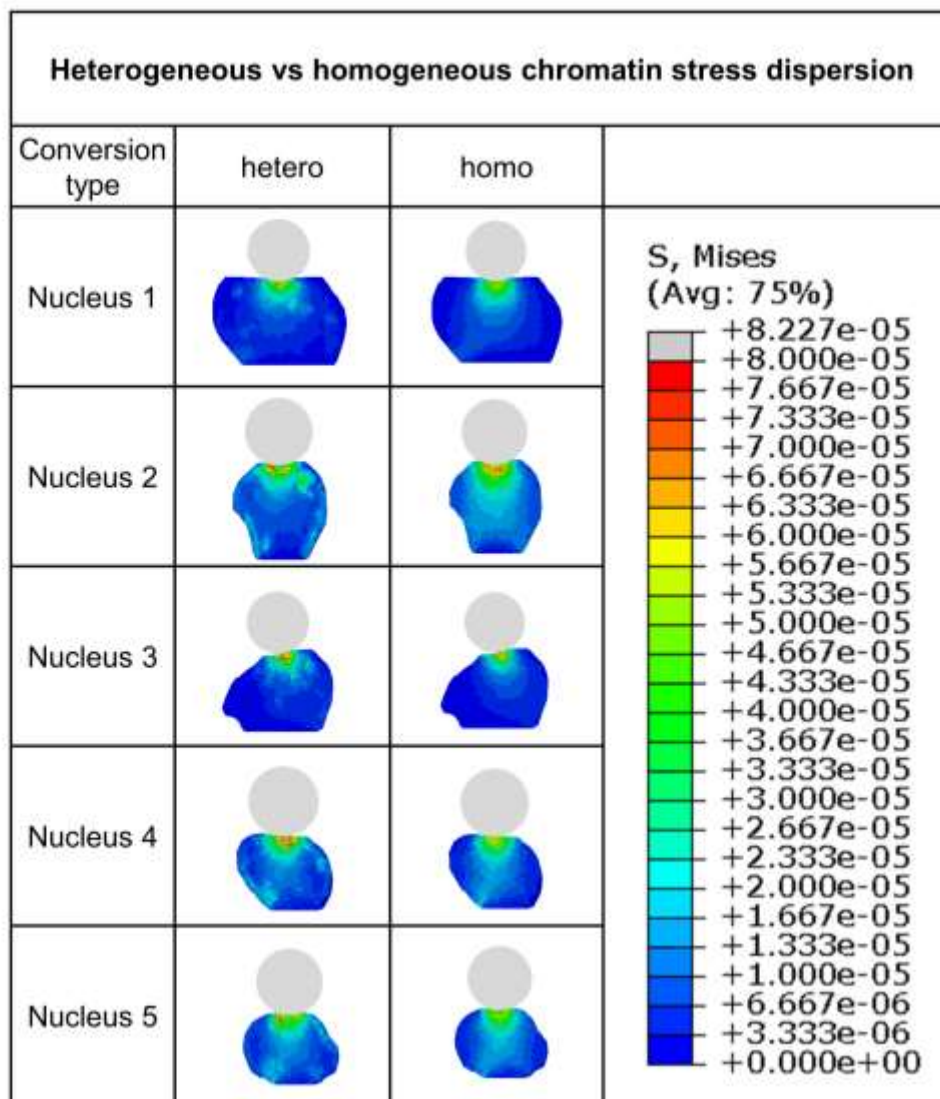


Figure S4. Heterogeneous vs homogeneous stress dispersion.

Nuclei models 1-5 were created with optimized heterogeneous and homogeneous conversion factors. The nucleus models then underwent a simulated atomic force microscopy experiment with nucleus cross sections for the heterogeneous nuclei showing stress dispersions dependent on the chromatin density within the original images (left) as well as homogeneous models showing a stress dispersion not dependent on the original chromatin density (right).

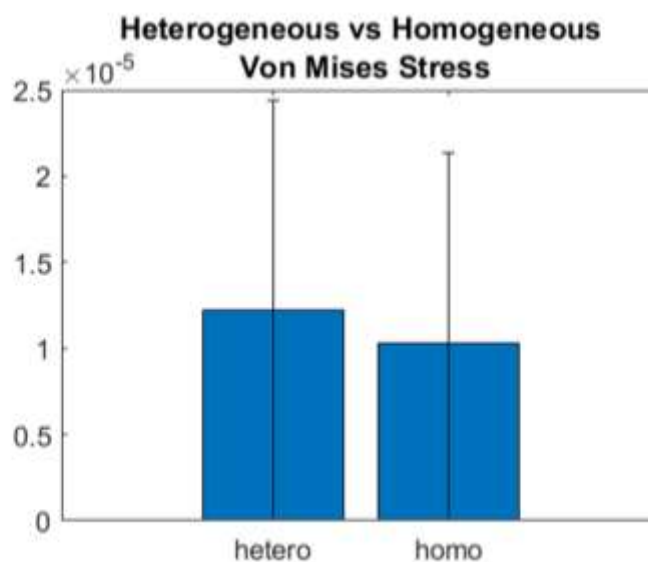


Figure S5. Von-mises stress comparison using stress from each element. Von-mises stress was taken from each element of the homogeneous and heterogeneous models of nuclei #4 and #5 and plotted above showing that the mean stress is similar between the two groups ($p > .05$).

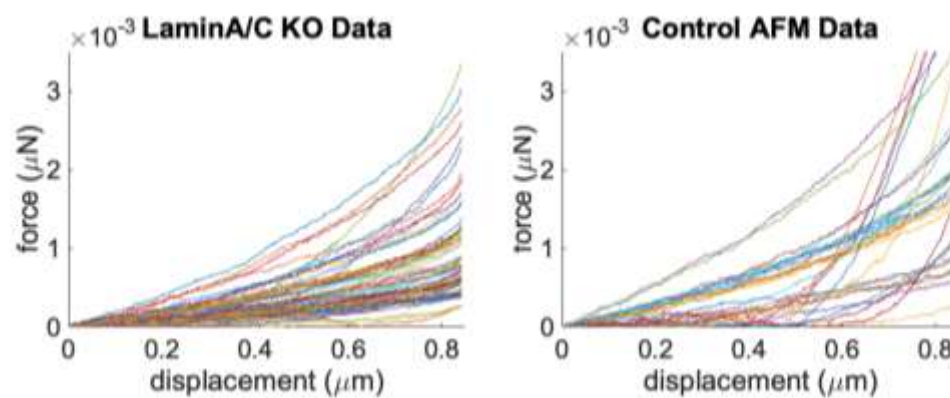


Figure S6. Atomic force microscopy curves. Atomic force microscopy experiment data for laminA/C knockdown nuclei (n=72, left) and control nuclei (n=30, right) has been plotted using Matlab.

CHAPTER FIVE: RESEARCH CONCLUSIONS AND FUTURE DIRECTIONS

5.1 Summary of research

The overarching goals of this research were to:

- Develop a framework of generating finite element models of the nucleus from the confocal microscopy scans of a nucleus that reflect specific nucleus geometry
- Tune these models to replicate real world performance of the nucleus while conserving heterochromatin geometry.
- Test the consistency of converting nucleus images into finite element models across different sets of images.

The significant results of this research include

- It is possible to generate models that reflect the geometry of the nucleus
- It is possible to create homogeneous models that mimic the results of both chromatin and laminA/C
- The exact conversion factors between image density and stiffness of the nucleus must be found cannot be found using the means posed within this research
- The heterogeneous material stiffness can replicate the performance of the homogeneous chromatin while creating different stress patterns
- Without the ability to get a solid set of conversion factors it is impossible to test how the conversion factors change between nucleus models

5.2 Current limitations

Our current research was limited by the correlation between b-c constants that was displayed within our *in silico* experiments. The ability for the nucleus to mimic the external mechanical response of a real world nucleus with an infinitely large amount of b-c conversion coefficients makes it impossible to narrow down a specific combination that best represents the image voxel intensity to stiffness for both the chromatin and LaminA/C of the nucleus. This makes it impossible to create realistic heterogeneous models of both chromatin and laminA/C within our research since it is impossible to deduce the proper b-c value combination for either material.

5.3 Future directions

For future versions of this research it is recommended that the conversion coefficients between image voxel intensity and elasticity be found by developing and using a phantom rather than to attempt to optimize *in silico* experiments to reflect real world data. It is then recommended that these coefficients be compared across different scans in order to find how consistent the microscopy scans used to make finite element models are across imaging sessions. Once this is done, this system can be utilized to generate finite element models of the nucleus in order to study the mechanical properties of isolated MSC nuclei using microscopy alone.

REFERENCES

1. Humphrey JD, Dufresne ER, Schwartz MA. Mechanotransduction and extracellular matrix homeostasis. *Nat Rev Mol Cell Biol.* 2014 Dec;15(12):802-12. doi: 10.1038/nrm3896. Epub 2014 Oct 22. Review. PubMed PMID: 25355505; PubMed Central PMCID: PMC4513363.
2. Peister, A. *et al.* Adult stem cells from bone marrow (MSCs) isolated from different strains of inbred mice vary in surface epitopes, rates of proliferation, and differentiation potential. *Blood* **103**, 1662-1668, doi:10.1182/blood-2003-09-3070 (2004).
3. Bas, G. *et al.* Low Intensity Vibrations Augment Mesenchymal Stem Cell Proliferation and Differentiation Capacity during in vitro Expansion. *Scientific reports* **10**, 9369, doi:10.1038/s41598-020-66055-0 (2020).
4. Koaykul C, Kim MH, Kawahara Y, Yuge L, Kino-Oka M. Alterations in Nuclear Lamina and the Cytoskeleton of Bone Marrow-Derived Human Mesenchymal Stem Cells Cultured Under Simulated Microgravity Conditions. *Stem Cells Dev.* 2019 Sep 1;28(17):1167-1176. doi: 10.1089/scd.2018.0229. Epub 2019 Jul 17. PubMed PMID: 31169056.
5. Lai RC, Yeo RW, Lim SK. Mesenchymal stem cell exosomes. *Semin Cell Dev Biol.* 2015 Apr;40:82-8. doi: 10.1016/j.semcd.2015.03.001. Epub 2015 Mar 9. Review. PubMed PMID: 25765629.
6. Hanna H, Mir LM, Andre FM. In vitro osteoblastic differentiation of mesenchymal stem cells generates cell layers with distinct properties. *Stem Cell Res Ther.* 2018 Jul 27;9(1):203. doi: 10.1186/s13287-018-0942-x. PubMed PMID: 30053888; PubMed Central PMCID: PMC6063016.

7. Touchstone, H. *et al.* Recovery of stem cell proliferation by low intensity vibration under simulated microgravity requires intact LINC complex *npj. Microgravity* **5**, doi:doi.org/10.1038/s41526-019-0072-5 (2019).
8. Martins RP, Finan JD, Guilak F, Lee DA. Mechanical regulation of nuclear structure and function. *Annu Rev Biomed Eng.* 2012;14:431–455.
doi:10.1146/annurev-bioeng-071910-124638
9. Lammerding J, Fong LG, Ji JY, Reue K, Stewart CL, Young SG, Lee RT. Lamins A and C but not lamin B1 regulate nuclear mechanics. *J Biol Chem.* 2006 Sep 1;281(35):25768-80. doi: 10.1074/jbc.M513511200. Epub 2006 Jul 5. PubMed PMID: 16825190.
10. “Finite Element Analysis Software.” *Autodesk*,
www.autodesk.com/solutions/finite-element-analysis.
11. “Tetrahedral Element.” *Tetrahedral Element - an Overview | ScienceDirect Topics*, ScienceDirect, www.sciencedirect.com/topics/engineering/tetrahedral-element.
12. “Mesh Refinement.” *Mesh Refinement - an Overview | ScienceDirect Topics*, ScienceDirect, www.sciencedirect.com/topics/engineering/mesh-refinement.
13. Alonso, José Luis, and Wolfgang H Goldmann. “Feeling the Forces: Atomic Force Microscopy in Cell Biology.” *Life Sciences*, vol. 72, no. 23, 25 Apr. 2003, pp. 2553–2560., doi:10.1016/s0024-3205(03)00165-6.
14. Zucco, Antonino. “Bonemat, Mapping CT Properties to Meshes.” *Bonemat*, Instituto Ortopedico Rizzoli, www.bonemat.org/.
15. Pagnotti, G. M. *et al.* Combating osteoporosis and obesity with exercise: leveraging cell mechanosensitivity. *Nature Reviews Endocrinology*, doi:10.1038/s41574-019-0170-1 (2019).
16. Engler, A. J., Sen, S., Sweeney, H. L. & Discher, D. E. Matrix elasticity directs stem cell lineage specification. *Cell* **126**, 677-689, doi:10.1016/j.cell.2006.06.044 (2006).

17. Andalib, M. N., Lee, J. S., Ha, L., Dzenis, Y. & Lim, J. Y. Focal adhesion kinase regulation in stem cell alignment and spreading on nanofibers. *Biochemical and biophysical research communications* **473**, 920-925, doi:10.1016/j.bbrc.2016.03.151 (2016).
18. Harris, A. R., Jreij, P. & Fletcher, D. A. Mechanotransduction by the Actin Cytoskeleton: Converting Mechanical Stimuli into Biochemical Signals. *Annual Review of Biophysics* **47**, 617-631, doi:10.1146/annurev-biophys-070816-033547 (2016).
19. Shiu, J.-Y., Aires, L., Lin, Z. & Vogel, V. Nanopillar force measurements reveal actin-cap-mediated YAP mechanotransduction. *Nature cell biology* **20**, 262-271, doi:10.1038/s41556-017-0030-y (2018).
20. Le, H. Q. *et al.* Mechanical regulation of transcription controls Polycomb-mediated gene silencing during lineage commitment. *Nature cell biology* **18**, 864-875, doi:10.1038/ncb3387 (2016).
21. Makhija, E., Jokhun, D. S. & Shivashankar, G. V. Nuclear deformability and telomere dynamics are regulated by cell geometric constraints. *Proceedings of the National Academy of Sciences of the United States of America* **113**, E32-40, doi:10.1073/pnas.1513189113 (2016).
22. Darling, E. M. & Di Carlo, D. High-Throughput Assessment of Cellular Mechanical Properties. *Annual review of biomedical engineering* **17**, 35-62, doi:10.1146/annurev-bioeng-071114-040545 (2015).
23. Ghosh, S. *et al.* Deformation Microscopy for Dynamic Intracellular and Intranuclear Mapping of Mechanics with High Spatiotemporal Resolution. *Cell reports* **27**, 1607-1620.e1604, doi:10.1016/j.celrep.2019.04.009 (2019).
24. Stephens, A. D., Banigan, E. J. & Marko, J. F. Separate roles for chromatin and lamins in nuclear mechanics. *Nucleus (Austin, Tex.)* **9**, 119-124, doi:10.1080/19491034.2017.1414118 (2018).

25. Stephens, A. D. *et al.* Chromatin histone modifications and rigidity affect nuclear morphology independent of lamins. *Molecular biology of the cell* **29**, 220-233, doi:10.1091/mbc.E17-06-0410 (2018).
26. Sankaran, J. S. *et al.* Knockdown of formin mDia2 alters lamin B1 levels and increases osteogenesis in stem cells. *Stem Cells* **38**, 102-117, doi:10.1002/stem.3098 (2020).
27. Tang, G., Galluzzi, M., Zhang, B., Shen, Y. L. & Stadler, F. J. Biomechanical Heterogeneity of Living Cells: Comparison between Atomic Force Microscopy and Finite Element Simulation. *Langmuir : the ACS journal of surfaces and colloids* **35**, 7578-7587, doi:10.1021/acs.langmuir.8b02211 (2019).
28. Rubin, J., Styner, M. & Uzer, G. Physical Signals May Affect Mesenchymal Stem Cell Differentiation via Epigenetic Controls. *Exercise and sport sciences reviews* **46**, 42-47, doi:10.1249/jes.0000000000000129 (2018).
29. Dupont, S. *et al.* Role of YAP/TAZ in mechanotransduction. *Nature* **474**, 179-183, doi:http://www.nature.com/nature/journal/v474/n7350/abs/10.1038-nature10137-unlocked.html#supplementary-information (2011).
30. Wang, L., Wang, L., Xu, L. & Chen, W. Finite Element Modelling of Single Cell Based on Atomic Force Microscope Indentation Method. *Computational and Mathematical Methods in Medicine* **2019**, 7895061, doi:10.1155/2019/7895061 (2019).
31. McGarry, J. G. & Prendergast, P. J. A three-dimensional finite element model of an adherent eukaryotic cell. *European cells & materials* **7**, 27-33; discussion 33-24 (2004).
32. Heo, S. J. *et al.* Biophysical Regulation of Chromatin Architecture Instills a Mechanical Memory in Mesenchymal Stem Cells. *Scientific reports* **5**, 16895, doi:10.1038/srep16895 (2015).